Research Article

Received: 27 January 2023 Revised: 29 April 2023 Accepted article published: 9 May 2023 Published online in Wiley Online Library: 18 May 2023

(wileyonlinelibrary.com) DOI 10.1002/jctb.7423

Recyclable functionalized polyethyleneimine-coated magnetic nanoparticles for efficient removal of lead from aqueous solutions

Chimaine F Tsague,[a,b] Hanna S Abbo,[a,c] Divine M Yufanyi,[d] Agwara M Ondoh[b] and Salam JJ Titinchi[a*]

Abstract

Background: Lead is among the most lethal heavy metals, displaying toxicity towards humans, animals and plants. Removal of lead ions from wastewater prior to its disposal is very important. Consequently, the development of adsorbents which can effectively remove Pb(II) from water is a subject of growing research interest.

Results: Polyethyleneimine-coated magnetic nanoparticles functionalized with various compounds, namely salicylaldehyde, carbon disulfide and *o*-vanillin, were synthesized and employed in the removal of Pb(II) from aqueous solutions. These compounds act as chelating agents which bind to toxic metal ions to form complex structures which are easily removed from the solutions. A very effective uptake of Pb(II) (98.1% of 25 mg L^{-1} Pb(II)) was achieved with an adsorbent dose of 10 mg, a contact time of 60 min and at a pH of 6.5. Equilibrium data for isothermal, kinetic and thermodynamic studies indicate that the process of adsorption fitted well with the Langmuir adsorption isotherm model. The kinetics of adsorption proceeded through a pseudo-second-order rate while the thermodynamic parameters indicated that the process was spontaneous and endothermic.

Conclusion: Functionalization of iron oxide nanoparticles was confirmed by various techniques. Adsorption factors were optimized in order to achieve maximum removal of Pb(II). The modified magnetic materials are highly effective active sorbent materials. The hydroxyl, thiol and thiocarbamate groups have a synergistic effect on Pb^{2+} removal through electrostatic interactions and chelation. Adsorption studies demonstrate that a high adsorption capacity (92%) was achieved within 10 min at 25 °C using the adsorbent MNP@PEI-CS_2. The nanoadsorbents can be reused without affecting their removal capacity.

Supporting information may be found in the online version of this article.

Keywords: heavy metals; removal; recovery; adsorption; wastewater

INTRODUCTION

A major contributor to the problems of water pollution are effluents from industrial wastewater discharge. On average, cities in developing countries generate between 30 and 70 mm^3 of wastewater per person per year.[1] The absence of facilities to treat wastewater has resulted in the emptying of effluents and wastewater into surface water sources, which also serve as dumping sites for domestic wastes resulting in further pollution.[2] Moreover, there is an upsurge in the release of poisonous wastes, comprising toxic chemicals such as heavy metals, due to industrialization.[3,4] Various surveys have shown that countries that are affected the most by pollution due to heavy metals are developing ones. Several different regulatory bodies, World Health Organization, Environmental Protection Agency and the Food and Agriculture Organization have established concentration boundaries for these metal ions in water. Concentrations beyond these boundaries are considered to be unsafe for humans and animals.[5] Complications to human health such as damage to the immune, central nervous and reproductive systems are some of the consequences of contact with heavy metal ions.[3] A major challenge to numerous countries in the world is groundwater contamination by heavy metals.[6] The heavy metal pollutants present in effluents are known to be non-biodegradable and can accumulate in living organisms through the food chain.[7]

The toxicity of most of these heavy metals is known. They are dangerous to tissue and organs and can be carcinogenic at low concentrations, thus putting human health, animals, plants and urban ecosystems at risk. Lead (Pb) is among the most lethal heavy metals, displaying toxicity towards humans (target organs

* *Correspondence to: SJJ Titinchi, Department of Chemistry, University of the Western Cape, Cape Town, 7535, South Africa, E-mail: stitinchi@uwc.ac.za*

a *Department of Chemistry, University of the Western Cape, Cape Town, South Africa*

b *Department of Chemistry, University of Yaoundé I, Yaoundé, Cameroon*

c *Department of Chemistry, College of Science, University of Basrah, Basrah, Iraq*

d *Department of Fundamental Science, Higher Technical Teacher Training College, University of Bamenda, Bambili, Cameroon*

being the liver, kidney, central nervous system and the brain), animals and plants. Lead is lethal to several key body organs such as the brain, the liver, the kidney and the nervous system.[8] The main sources of lead pollution are anthropogenic which include the manufacture of batteries, acid metal plating and ceramic and glass industries. Thus, elimination of lead ions from wastewater prior to its disposal is very important. Consequently, development of methods which can effectively remove Pb(II) from water is a subject of growing research interest. Amongst the numerous methods reported for the removal of Pb(II) are chemical treatment, reverse osmosis,[9] coagulation and flocculation,[10] ion exchange,[11] oxidation and membrane separation,[12] chemical precipitation[5] and adsorption.[13] Nevertheless, all these methods are limited by procedures that are time-consuming, requiring expensive equipment and/or the need for continuous chemical refill.

Flexibility of design, ease of operation, easy handling, reuse of the same adsorbents and in several instances the generation of high-quality treated effluents render the process of adsorption more efficient and economical.[14] For an adsorbent to be effective in removing large amounts of contaminant in a short time, it should have a large surface area, small diffusion, good resistance and rapidly attain equilibrium during adsorption. In addition, it should produce the least amount of sludge. It is thus significant in practical engineering applications to develop adsorbents with high surface areas and a small diffusion resistance.[15] This has been a subject of intensive research, resulting in several different materials such as activated carbon, zeolites and biomaterials all of which have been employed as adsorbents for heavy metal ion removal from wastewater. Nevertheless, disadvantages such as low capacity of adsorption, extended time of adsorption, as well as difficult and expensive processes (filtration, centrifugation) for adsorbent removal after the adsorption all serve to limit their large-scale application in water treatment.[16,17]

Recent developments in nanotechnology have led to nanoscale materials attracting increasing scientific attention for tackling environmental problems.[3] Though a variety of nanosized adsorbents are known, iron oxides (magnetic nanoparticles, MNPs), for example magnetite (Fe_3O_4), maghemite (γ-Fe_2O_3) and hematite (α-Fe_2O_3), have been extensively employed to remove heavy metals from water and wastewater samples.[18,19] Traditional adsorbents, in comparison to nanosized iron oxides, are cost-effective, easy to synthesize and environmentally benign, with large surface areas as well as being highly efficient. Magnetic iron oxide nanoparticles can also be easily recovered or manipulated with an external magnetic field.[20] However, the decrease in size of the metal oxide from the micrometer to the nanometer range alongside an increase in energy at their surfaces unavoidably leads to a decrease in their stability. Consequently, a tendency of these nanosized metal oxides is that of agglomeration due to van der Waals forces or other interactions, resulting in a significant decrease or loss of the high capacity or selectivity of these oxide particles. Furthermore, the extreme drops in pressure (or the difficulty in separating from aqueous systems) coupled with poor mechanical strength have rendered these oxide particles impracticable in systems with fixed beds or those with flow-through.[18] Depositing a polymer shell on the nanoparticles as well as dispersing the nanoparticles into materials that are probably porous (for example, diatomite or activated carbon that is in powder form) are some of the techniques which have been employed to prevent the formation of aggregates.[21] In order to circumvent such limitations, surface modification of iron oxide nanoparticles with appropriate nitrogen- or sulfur-containing polymeric ligands is imperative to improve interactions that are soft–soft in nature between heavy metal ions and active sites as well as to decrease the interference of hard cations such as alkaline earth metal ions.[22]

Cationic polymers, especially polyethyleneimine (PEI), have been extensively used for the delivery of genes owing to the charge on their surfaces being highly positive, thus permitting electrostatic interactions with centers of negative charge.[23] PEI, a polyamine, is a hydrophilic polymer which is soluble in water and contains many nitrogen atoms in the amino groups on its molecular chains. Based on the structure, it can be classified as either linear- or branched-chain PEI. Linear PEI contains secondary amine groups, while branched PEI contains amino groups that are primary, secondary and tertiary.[24] The assumption that composites derived from PEI and MNPs demonstrate both the magnetic properties of MNPs and the very high adsorption capacity of PEI has resulted in the scientific exploration of MNPs modified by PEI (MNP@PEI), prepared through diverse synthetic techniques including electrostatic interaction, self-assembly, dispersion polymerization and coprecipitation.[25]

In this paper, we present a simple hydrolysis route for preparing a new generation of magnetically separable adsorbents decorated with new functional groups to reach high stability and adsorption capacity. MNPs were first coated with PEI by covalently grafting PEI on the surfaces of Fe_3O_4 followed by functionalization with organic and inorganic compounds (salicylaldehyde, *o*-vanillin and carbon disulfide) having various electron donor sites, i.e. N and O or S. These adsorbents were employed in Pb(II) ion removal from aqueous solution and the concentration of metal ions adsorbed was determined by atomic absorption spectrometry (AAS). Coating and functionalization of Fe_3O_4 not only render the adsorbents hydrophilic leading to a reduction of adsorption during wastewater treatment but also equally provide several hydroxyl, thiol and thiocarbamate groups, which may act in synergy to coordinate or chelate the Pb(II) metal ions. Consequently, this increases their absorption capacity more rapidly and may easily be removed from the solution.

The proposed mechanism of formation of the materials is presented and discussed. Furthermore, the effects of different parameters including the concentration of Pb(II) ions, contact time, pH and the amount of adsorbent on the capacity of adsorption of Pb(II) ions by the prepared nanocomposites were explored. The reusability as well as adsorption mechanism of Pb(II) ions were also evaluated.

EXPERIMENTAL

Chemicals

Ferrous sulfate heptahydrate ($FeSO_4{\cdot}7H_2O$, 99.5%), potassium hydroxide (99%), potassium nitrate (99%), sodium hydroxide (98%), hydrochloric acid (37%), absolute ethanol, PEI (branched, average molecular weight ~ 25 000 g mol^{-1}), carbon disulfide (CS_2), salicylaldehyde (SAL), *o*-vanillin (OV) and lead standard solution (1000 ppm) were obtained from Sigma-Aldrich and were used as supplied.

Synthesis of magnetic iron oxide nanoparticles

MNPs were prepared by a hydrolysis method reported by Lin *et al.* with slight modifications.[26] Fe(II) solution was prepared by dissolving $FeSO_4{\cdot}7H_2O$ (5 g, 18 mmol) in 35 mL of deionized water under a nitrogen atmosphere (solution A). In a separate flask, KNO_3 (0.4053 g, 14.6 mmol) and KOH (2.8075 g, 50 mmol) were

dissolved in 15 mL of deionized water (solution B). At 90 °C, solution B was added dropwise (5 min) to solution A under continuous stirring to give a black solution. The solution was maintained in an oil bath at 90 °C for 1 h to ensure homogeneity. The MNPs were separated from the reaction mixture using a magnet. The Fe_3O_4 MNPs collected were rinsed a number of times with deionized water until the pH became neutral and then dried in an oven.

Preparation of PEI-coated MNPs

The electrostatic adsorption of PEI onto the surfaces of Fe_3O_4 (MNPs) was achieved through the procedure of Aeineh *et al.* with some modifications.[27] In a nitrogen atmosphere, PEI (200 mg) and Fe_3O_4 MNPs (100 mg) were dispersed in deionized water (20 mL) with vigorous stirring, while raising the temperature of the mixture to 90 °C for 3 h. The precipitate formed was magnetically separated, washed many times with deionized water to eliminate excess PEI and dried in a vacuum oven.

Functionalization of PEI-coated MNPs with organic compounds

Salicylaldehyde-functionalized PEI-coated MNPs

MNP@PEI was functionalized with salicylaldehyde according to a reported procedure.[28] Excess salicylaldehyde (1 mL, 9.58 mmol) was added to a 100 mL suspension of MNP@PEI (2 g) in absolute ethanol, and the mixture was heated under reflux for 8 h. The modified nanoparticles obtained were washed thrice with deionized water, then with ethanol, and dried at ambient temperature. The obtained material was designated as MNP@PEI-SAL. Scheme 1 illustrates the preparation.

Carbon disulfide-functionalized PEI-coated MNPs

The surface of MNP@PEI was modified with carbon disulfide according to a reported method.[26] Into a reaction mixture containing 20 mL of 0.1 mol L^{-1} NaOH, 4 mL of 2-propanol and 0.3 mL of CS_2 was added MNP@PEI (1 g). The reaction mixture was left stirring for 6 h. The product obtained was separated using an external magnet, washed with 2-propanol and dried at room temperature. The obtained material was designated as MNP@PEI-CS_2 (Scheme 1).

o-*Vanillin-functionalized PEI-coated MNPs*

A mixture of 1 g of *o*-vanillin in absolute ethanol (30 mL) was added to 0.5 g of MNP@PEI in 20 mL of ethanol, which had previously been sonicated. The suspension was heated under reflux at 70 °C for 3 h. The product was isolated by magnetic separation, washed thrice with ethanol and dried at 80 °C in an oven. The obtained material was designated as MNP@PEI-OV (Scheme 1).

Adsorption tests

Pb(II) ions were adsorbed onto the as-prepared adsorbents, at room temperature, using a batch method. In a given process, a known mass of the adsorbent (2–15 mg) was added to a test tube containing 50 mL of aqueous solution at room temperature with different initial concentrations of Pb(II) ions (25, 50 and 100 ppm), pH values (2.5–8.5) and for various contact times (10–120 min).

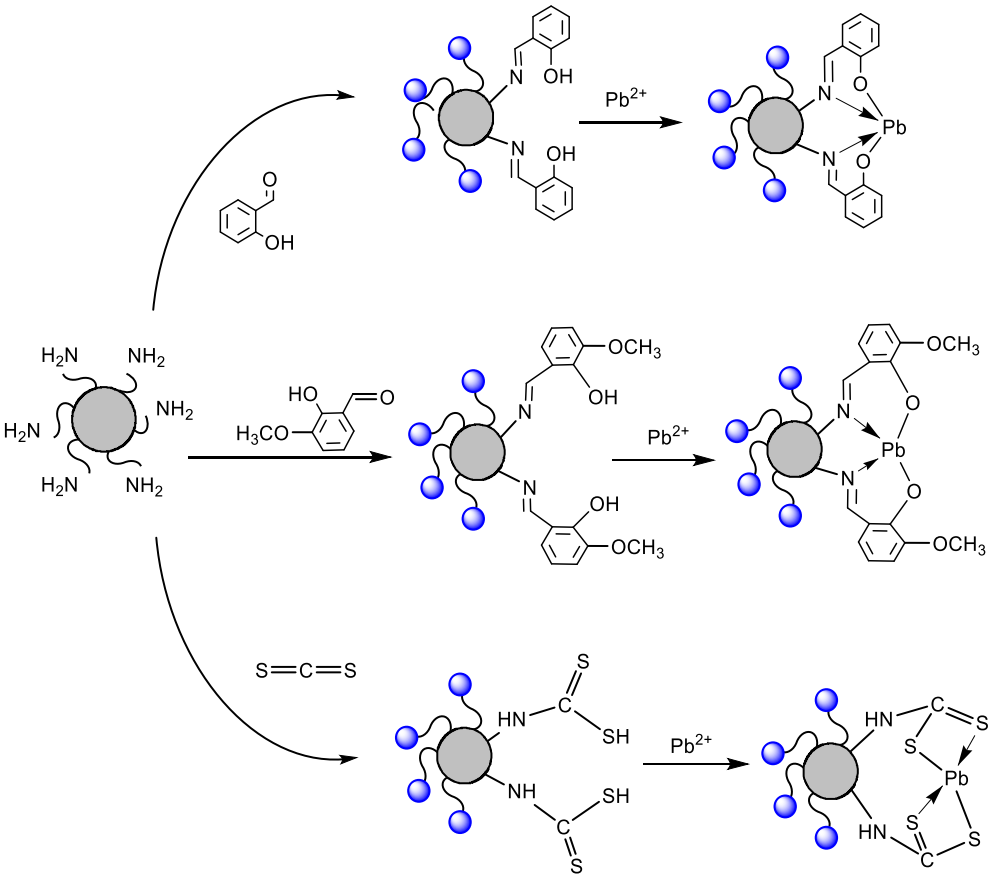

Scheme 1. Synthesis route for the functionalized PEI-coated MNPs, namely MNP@PEI-CS_2, MNP@PEI-SAL, MNP@PEI-OV, and the adsorption of Pb(II) ions by these adsorbents.

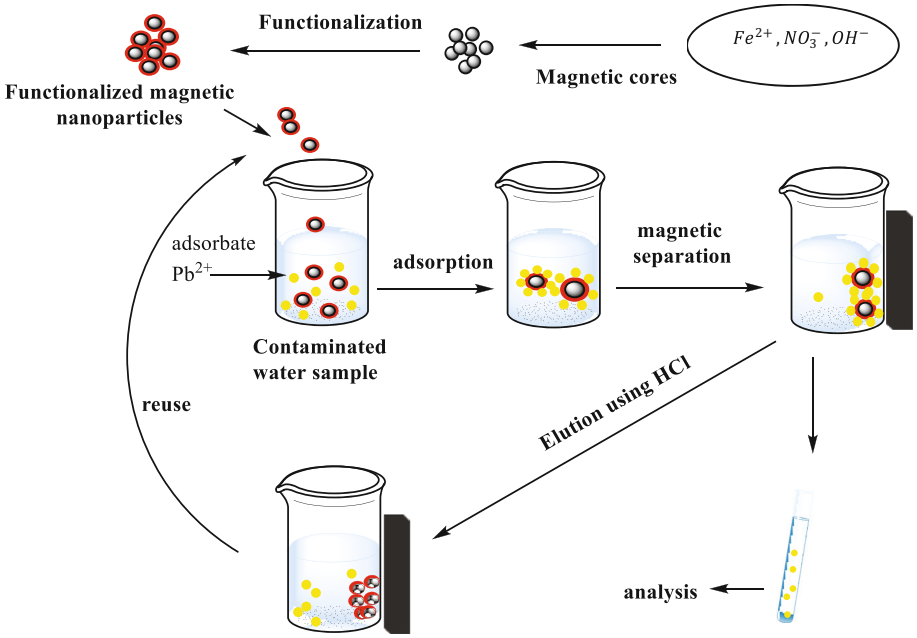

Scheme 2. Schematic representation of aqueous solution purification adsorption/regeneration cycle.

The solution was stirred at 4 rpm and left for a certain contact time. After a specific interval of time, a 1 mL aliquot was withdrawn and the adsorbent was separated using a magnet and diluted to 4 mL with deionized water (Scheme 2). To determine the adsorption capacities of the synthesized materials, AAS was used to measure the concentration of Pb(II) ions detected/available after the adsorption process. The removal efficiency (RE) and the equilibrium adsorption capacity (q_e (mg g^{-1})) were evaluated using Eqns (1) and (2):

$$\mathrm{RE}\,(\%) = \frac{C_o - C_t}{C_o} \times 100 \quad (1)$$

$$q_e = \frac{(C_o - C_e) \times V}{W} \quad (2)$$

where C_o and C_t (mg L^{-1}) are the concentrations of Pb(II) solution at the initial time and at time t (min), respectively, q_e represents the equilibrium adsorption capacity of the adsorbent (mg g^{-1}), V is the volume of the solution (L) and W is the weight of the adsorbent used (g).

The kinetics of Pb(II) ion adsorption was investigated using the same procedure as described above. Different contact times (10–120 min) at the optimum amounts of adsorbent dosage, pH and initial concentration of Pb(II) solution, at room temperature, were employed. With regards to the kinetics of adsorption, the capacity q_t of the adsorbents to adsorb Pb(II) at time t can be determined from Eqn (3):

$$q_t = \frac{(C_o - C_t) \times V}{W} \quad (3)$$

where q_t is the adsorption capacity (mg g^{-1}) at time t and C_t is the concentration (mg L^{-1}) of the Pb(II) at time t.

Adsorption isotherms at different concentrations of Pb(II) ion solutions (2, 4, 6, 8, 10, 15 mg L^{-1}) were studied using the same procedure as above. The solution pH (adjusted using 0.1 mol L^{-1} NaOH or HCl solution), contact time and adsorbent dosage were adjusted to their optimum values obtained from the batch optimization procedure, i.e. pH 6.5, 60 min and 10 mg, at room temperature.

The effects of changes in temperature on the adsorption were determined at 295, 308, 318, 328 and 338 K. Thermodynamic studies were carried out at these same temperatures according to the optimized conditions, at an adjusted contact time of 90 min.

To ascertain if the data collected were accurate, reliable and reproducible, mean values have been reported for the batch experiments which were done in triplicate.

Structural and chemical characterization of nanoparticles

Fourier transform infrared (FTIR) spectra were recorded with a PerkinElmer FTIR spectrophotometer (Spectrum100) using the KBr pellet technique from 4000 to 400 cm^{-1}. Thermogravimetric analysis (TGA) was conducted in an atmosphere of nitrogen (20 mL min^{-1}), between 30 and 700 °C, at a heating rate of 10 °C min^{-1}, using a PerkinElmer Simultaneous Thermal Analyzer (STA 6000). Scanning electron microscopy (SEM) images were obtained with a Zeiss Auriga field emission gun SEM instrument. High-resolution transmission electron microscopy (TEM) was performed using an FEI Technai G2F20 X-Twin MAT field emission microscope. Powder X-ray diffraction (XRD) patterns were recorded using a D8 Advance Bruker AXS X-ray diffractometer with Bragg–Brentano geometry and a Cu-Kα source (40 kV, 40 mA).

Regeneration and reusability study

To determine the material after the adsorption process, the amount of heavy metals desorbed from the adsorbents was evaluated to assess the capacity of the materials to be regenerated and reused in an acidic medium. Consecutive sorption and desorption cycles were studied in triplicate. In 50 mL of Pb(II) ion solution (25 ppm), 10 mg of MNP@PEI-CS_2 was added and stirred for an hour. After recording the final Pb(II) ion concentration at equilibrium using AAS, the materials were collected, washed many times with deionized water to ensure the removal

of unbound heavy metal and then treated with 25 mL of 0.1 mol L^{-1} HCl solution (pH ≈ 1.5). After desorption, the magnetic materials were recovered and washed many times with deionized water until neutral pH (6.5–7) and then dried in an oven.

RESULTS AND DISCUSSION

Synthesis and structure of MNP@PEI-SAL, MNP@PEI-CS_2 and MNP@PEI-OV nanomaterials

The magnetic Fe_3O_4 core of the adsorbent was obtained through a hydrolysis method. PEI was coated, by electrostatic absorption, onto the surfaces of Fe_3O_4 through conventional sol–gel methods. These nanomaterials were further functionalized with organic compounds salicylaldehyde, *o*-vanillin and carbon disulfide, through condensation reactions of the NH_2 groups on PEI with carbonyl and thiol groups of the functionalization materials (Scheme 1).

FTIR characterization

To identify the functional groups at the surfaces of the pristine and the functionalized MNPs as well as to check their chemical compositions, FTIR spectra of the samples were obtained from 4000 to 400 cm^{-1}, as shown in Fig. 1. The characteristic peaks for pure Fe_3O_4 MNPs appeared at 3406 and 580 cm^{-1}. The strong and sharp peak at 580 cm^{-1} is attributed to Fe—O stretching vibration of the MNPs. The broad absorption band centered at 3406 cm^{-1} was assigned to the stretching vibration of O—H bonds of hydroxyl groups.[29,30] After coating with PEI, the new strong peaks that appeared at 2882–2949 cm^{-1} and the peak at 1082 cm^{-1} were attributed to aliphatic C—H vibrations and C—N stretching vibrations, respectively. This indicates the presence of PEI on the surface of Fe_3O_4 MNPs.[27] After reaction with the functionalization materials, the new absorption band that appeared at 1622 cm^{-1} in the spectrum of MNP@PEI-SAL was attributed to C═N stretching vibration. Weak bands at 1400–1500 cm^{-1} were attributed to C—C stretching vibrations of the aromatic ring.[28] The band at 1141 cm^{-1} can be attributed to the phenolic C—O bending vibration and the weak-intensity bands at 2883 and 2985 cm^{-1} to CH— stretching vibrations.[30] In the FTIR spectrum of MNP@PEI-OV (Fig. 1(D)), the characteristic band at 1630 cm^{-1} is an indication of C═N stretching mode and that at 3432 cm^{-1} was assigned to the O—H stretching vibration.[31] The spectrum of MNP@PEI-CS_2 (Fig. 1(E)) contains bands assigned to the thiouride moiety at 1450–1550 cm^{-1}.[32] Frequencies between those of C—N (1250–1350 cm^{-1}) and C═N (1632 cm^{-1}) bonds indicate that a partial double-bond character exists and the consequent delocalization of π-electron density on the dithiocarbamate group.[33] The band at 2380 cm^{-1} was assigned to S—H stretching vibrations.[34] Characteristic bands for dithiocarbamate (νC—S) vibrations at 950–1050 cm^{-1} indicate a unidentate or bidentate coordination mode of the dithiocarabamate ligand.[35] In this work, the presence of only one band (νC—S) observed around 1005 cm^{-1} suggests that the dithiocarbamate ligand coordinates in a bidentate manner.[36]

SEM–energy dispersive X-ray spectroscopy (EDS)

The morphologies of the naked MNPs and the coated materials MNP@PEI and MNP@PEI-CS_2 were investigated by SEM and selected area electron diffraction (SAED). SEM images (Fig. 2) indicate that the spinel-shape morphology of the nanomaterials does not change upon coating and functionalization. The composition of the as-prepared nanoparticles was confirmed by EDS (Fig. 2). The results indicate that the synthesized materials were mainly composed of Fe, C and O, except for MNP@PEI-CS_2 where the presence of S (0.17%) was also indicated. This confirms the successful functionalization of magnetite nanoparticles.

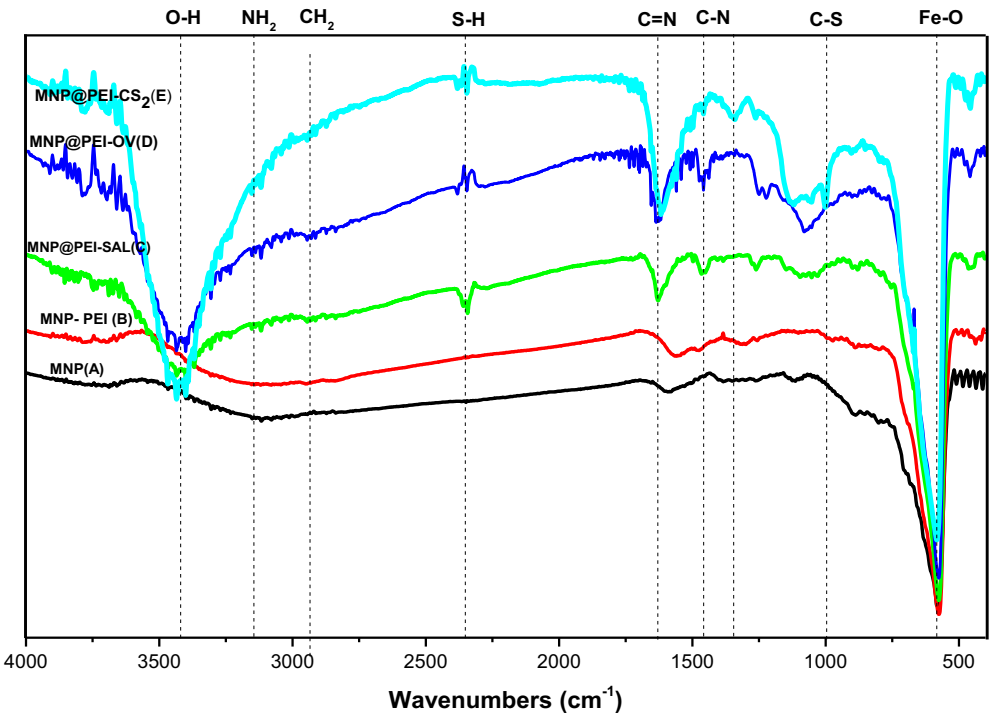

Figure 1. FTIR spectra of (A) MNPs, (B) MNP@PEI, (C) MNP@PEI-SAL, (D) MNP@PEI-CS_2 and (E) MNP@PEI-OV.

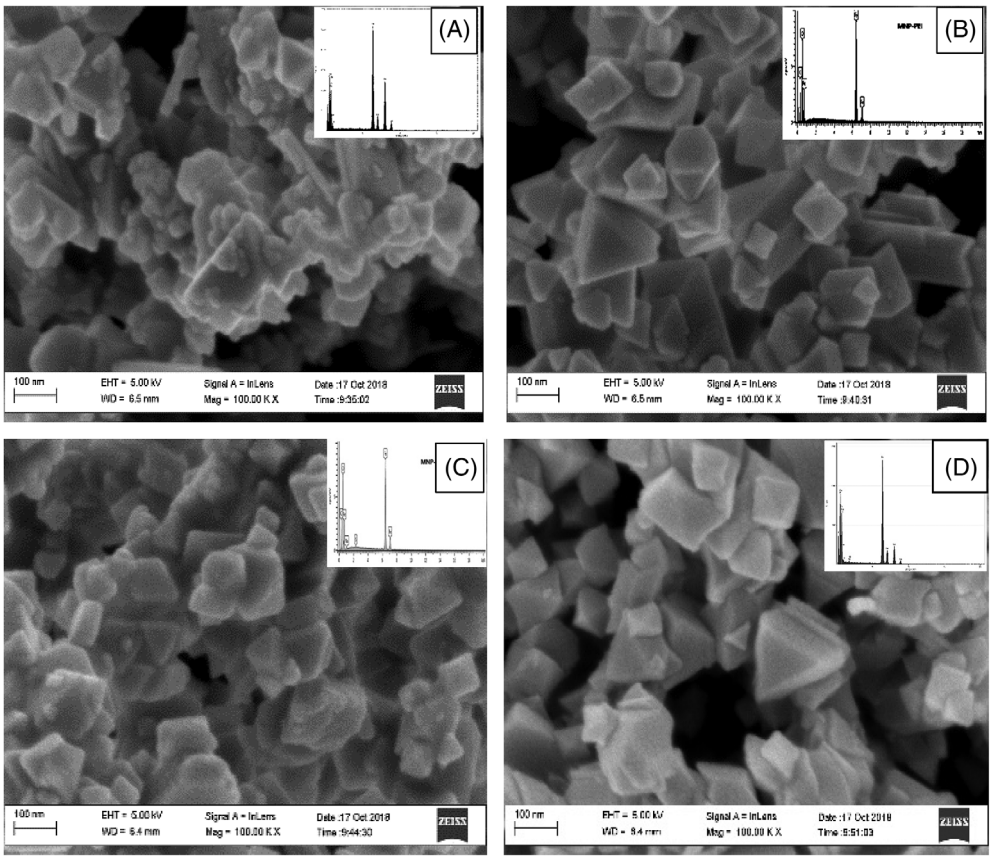

Figure 2. SEM images and EDS spectra of (A) MNPs, (B) MNP@PEI, (C) MNP@PEI-CS_2 and (D) MNP@PEI-SAL.

TEM/SAED

On the other hand, the TEM images (Fig. 3) show the morphology and structure of the Fe_3O_4 MNPs before and after coating with PEI and functionalizing by CS_2, as an example. The TEM images show that the naked and functionalized MNPs show smooth surfaces with good crystallinity. The crystallite size ranges from 20 to 40 nm, with an average crystallite size of most of the particles being *ca* 30 nm in diameter.

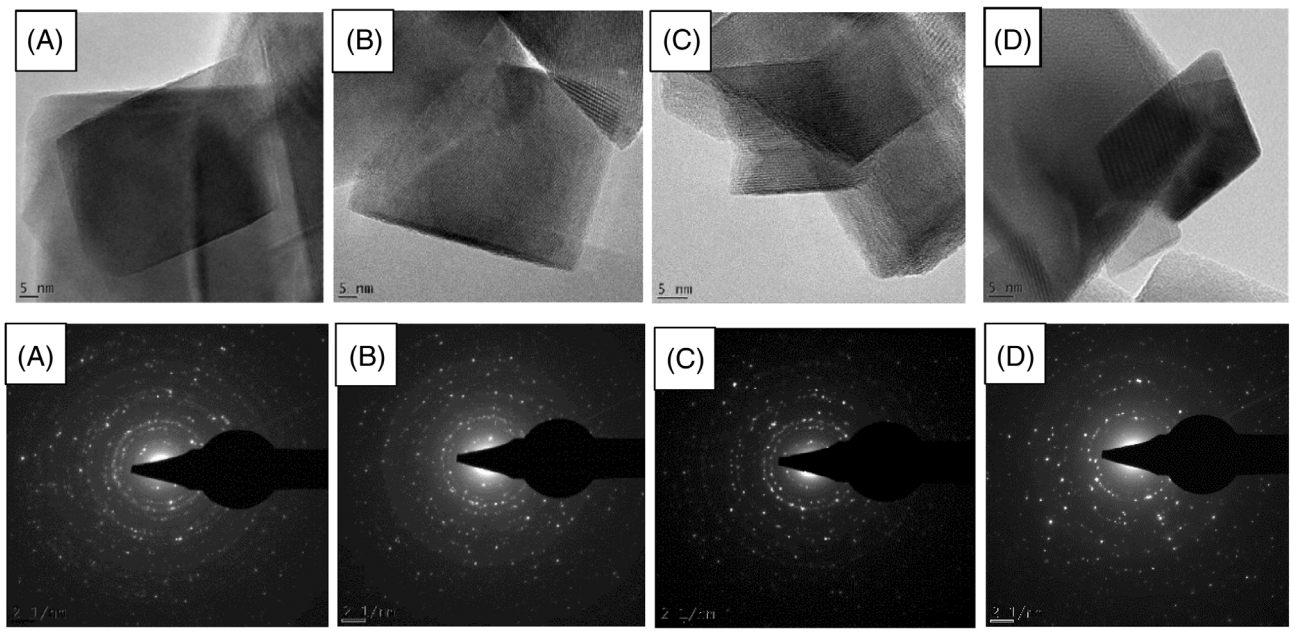

Figure 3. TEM images (top) and SAED patterns (bottom) of (A) MNPs, (B) MNP@PEI, (C) MNP@PEI-CS_2 and (D) MNP@PEI-SAL.

The SAED results (Fig. 3) further confirm that the phases of the MNPs were crystalline. The electron diffraction patterns of the coated and the functionalized materials were clear and well defined indicating that the MNPs were highly polycrystalline in nature.[37,38] These patterns could be indexed to the spinel form of Fe_3O_4. The diffraction rings found in the SAED pattern of the MNPs (Fig. 3) of the Fe_3O_4 phase can be indexed to the (311), (220), (400), (422), (511), (440) and (533) reflections from the crystal planes. These results match the XRD results (discussed below).

Powder XRD patterns

The powder XRD patterns of the prepared nanomaterial (Fig. 4) show well-defined peaks at 30°, 35°, 43°, 53°, 57°, 62° and 89° which can be indexed to the 220, 311, 400, 422, 511, 440 and 731 reflections of Fe_3O_4, respectively. These peaks match those of a spinel-type structure for Fe_3O_4 MNPs (JCPDS card no. 00-019-0629). The lattice constant $a = 8.396$ Å for these samples compares favorably with that of magnetite (8.39 Å). The strongest reflection peak is the (311) plane which is characteristic of a spinel structure.[39] Furthermore, there are no shifts in peaks observed in the powder PXRD patterns upon coating and functionalization, indicating that there was no change in the crystallinity and the stability of the core Fe_3O_4 MNPs due to surface modification.[40,41] While the well-developed peaks at some angles with sharp peak intensities indicate the crystallinity of the samples. Broad peaks, on the other hand, indicate that the particles are fine.

The crystallite size of the naked magnetite nanoparticles and the functionalized materials can be calculated using the Scherrer equation:

$$D = \frac{K\lambda}{\beta \cos\theta} \tag{4}$$

where λ is the wavelength, β is the peak width at half maximum and θ denotes the Bragg diffraction angle. The Scherrer constant $K = 0.89$ nm was used to obtain the crystallite size for all the materials. The average crystallite sizes of MNP, MNP@PEI, MNP@PEI-CS_2, MNP@PEI-SAL and MNP@PEI-OV were calculated according to the equation and found to be *ca* 24 nm.

Thermogravimetric analysis

The TGA profiles of the adsorbents MNP, MNP@PEI, MNP@PEI-SAL, MNP@PEI-CS_2 and MNP@PEI-OV along with the weight percentage loss are presented in the supporting information (Fig. S1). The naked Fe_3O_4 nanoparticles show a loss in weight of only *ca* 3% at temperatures below 150 °C which is assigned to the loss of physically adsorbed water molecules. The thermal decomposition of all the functionalized MNP adsorbents occurs in two steps in a wide temperature range (40–600 °C).[42] The weight loss in the first step (2–4%) starts shortly after increasing the temperature and continues until 150 °C. This is due to the presence of adsorbed water molecules though all adsorbents were dried at 150 °C for several hours.

MNP@PEI exhibited a weight loss of *ca* 1.5% between 150 and 400 °C which corresponds to the decomposition of PEI and leveled off after 400 °C indicating that the coated PEI polymeric layer had completely decomposed.[43] The percentage PEI loading was found to be 0.9%.

On the other hand, the functionalized nanoparticles, MNP@PEI-CS_2, MNP@PEI-SAL MNP@PEI-OV, showed a second decomposition step between 150 and 600 °C with weight losses of 0.9%, 3.9% and 6.3%, respectively. This step consists of overlapping steps and is due to the loss of PEI layers and the ligand moieties.

The observed weight gain in the TGA of MNPs from 350 to 600 °C could be attributed to a series of processes including the rapid oxidation of nanoscale Fe_3O_4 to γ-Fe_2O_3, the conversion of γ-Fe_2O_3 to α-Fe_2O_3 and the oxidation of preoxidized Fe_3O_4.[44]

Study of adsorption process

Effects of pH

Amongst the critical parameters in the process of adsorption, which has an effect on the charge on the surfaces of the adsorbing material, is the pH of the solution.[45] Variations in the solution pH can have important consequences on the ability of the adsorbent to adsorb. Consequently, we investigated how changes in pH affect adsorption properties within the pH range 2.5–8.5, while keeping the concentration of adsorbate fixed (25 ppm), the weight of adsorbent at 10 mg and the contact time at 60 min. As the pH was increased from 2.5 to 8.5, it was observed that the efficiency of removal was also

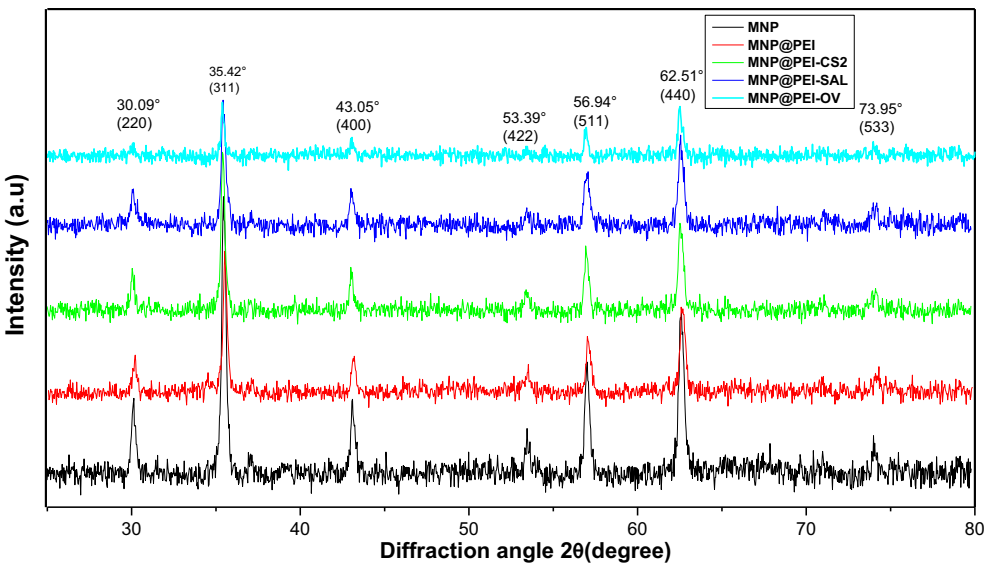

Figure 4. XRD patterns of MNPs, MNP@PEI, MNP@PEI-SAL, MNP@PEI-CS_2 and MNP@PEI-OV.

augmented as shown in Fig. 5(A). The efficiency of removal was found to be 5% at low pH values probably because hydrogen ion concentration was high in the solution which makes the adsorption sites positively charged, exerting a repelling effect on the Pb(II) cations and the adsorption process would thus be hindered.[46] At higher pH values, Pb(II) ions are converted to $Pb(OH)_2$, thus suppressing the adsorption of Pb ions and consequently there is a reduction of the removal efficiency.[47] The results indicated that the highest efficiency of Pb(II) ion removal was achieved at pH 6.5. Consequently, pH 6.5 was selected as the optimum pH of the medium.

Effect of adsorbent dosage

Four adsorbent amounts, 2, 5, 10 and 15 mg, were selected keeping all the other parameters constant: 25 ppm, pH 6.5 and contact time of 60 min. The selected adsorbent (MNP@PEI-CS_2) was added to 50 mL of a solution of Pb(II) ions while stirring. Increasing the amount of adsorbent from 2 to 15 mg led to a corresponding increase in the uptake of Pb(II), i.e. an increase of removal efficiency as shown in Fig. 5(B). The removal efficiency decreased slightly on using more than 10 mg of the adsorbent.[44,48] At a higher adsorbent amount (>10 mg), interactions between the binding sites of the adsorbent result in aggregation which could decrease the surface area. This phenomenon could explain the decrease in removal efficiency. Thus, the amount of adsorbent used subsequently in the analysis of Pb(II) ion removal was 10 mg.

Although at a higher adsorbent dosage there is a higher surface area, a higher number of active functional groups as well as active adsorption sites available,[43,47] interactions between the binding sites of the adsorbent resulting in aggregation and decrease in the available binding sites, at a higher adsorbent amount (>10 mg), could explain the decrease in removal efficiency.

Adsorption kinetics study

Effect of time of contact

Variation in the amount of Pb(II) ions removed with time using the as-prepared adsorbents is depicted in Fig. 6. It is shown that the efficiency of removal and adsorption capacity of Pb(II) ions increased as the contact time increased. This could be explained by the availability of several active binding sites on the adsorbing material coupled with the decrease in Pb(II) ion-occupied active sites as the time for adsorption increases. The maximum efficiency of removal of Pb(II) was 93.7% for MNPs, 94.4% for MNP@PEI, 95.1% for MNP@PEI-SAL, 98.1% for MNP@PEI-CS_2 and 94.35% for MNP@PEI-OV, after 60 min. As time progressed the surface coverage of the adsorbent was high, and no further adsorption took place after 60 min, and thus this time period was subsequently used in the study of the isotherms.

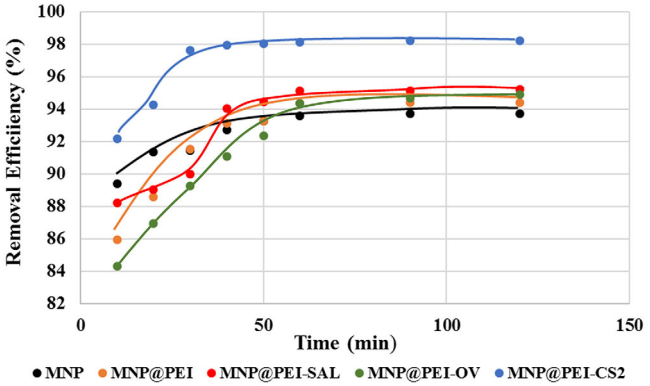

Figure 6. Removal efficiency of Pb(II) with time using various adsorbents.

The results demonstrated that MNP@PEI-CS_2 exhibited an excellent adsorption performance for Pb(II) compared to the other functionalized materials. Pb(II) is considered an intermediate ion based on the HSAB (hard–soft acid base) theory.[49] This can be elucidated to lead to a higher affinity towards sulfur, namely thiol functional group, than oxygen- and nitrogen-containing groups. This is due to thiol which is an electron-rich functional group and can form a chemical bond with Pb(II) ions due to the high affinity of Pb(II) for sulfur-based sorbents.[50]

Adsorption kinetic models

Isothermal adsorption equilibrium study

The process of adsorption is a dynamic equilibrium, and the rate of adsorption is a function of the physicochemical properties of the adsorbing material, the characteristics and concentration of the Pb(II) ions as well as the capacity of this metal ion to combine with the adsorbing material.[18] The proposed and accepted mechanism for removal of heavy metal ions from solutions using functionalized surface sorbents is adsorption. This mechanism is based on the chemical binding between O-, N- and S-containing groups and the heavy metal ion. The adsorption kinetics isotherms provide valuable insights into the reaction pathways and the mechanism of the adsorption process.[51] In the adsorption

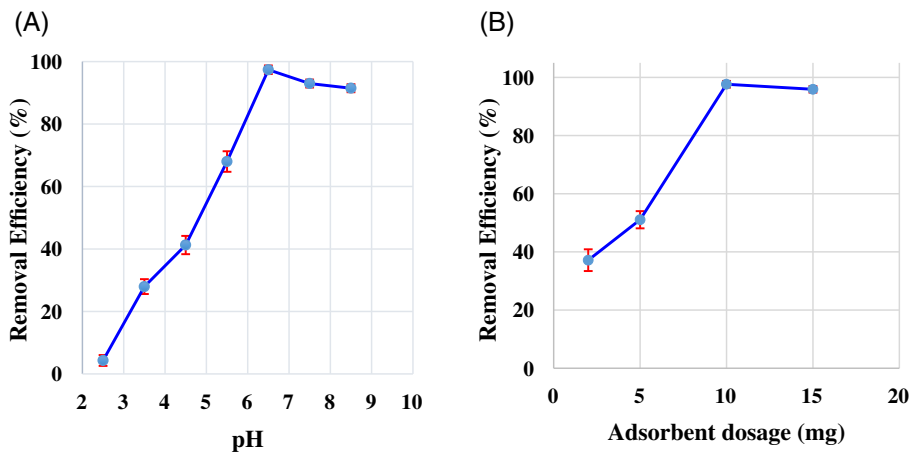

Figure 5. Effect of pH (A) and adsorbent dosage (B) on Pb(II) removal efficiency using MNP@PEI-CS_2.

mechanism a covalent and/or coordination bond is formed between the donor atoms of the functional group with metal ions. This behavior is further verified in the desorption process.

To investigate the rate and mechanism of adsorption of Pb(II) ions onto the MNPs, several kinetic models were performed/tested. Different kinetic equations (namely first order, second order, pseudo-first order, pseudo-second order and intraparticle diffusion) were tested to determine which model fits better with the experimentally obtained kinetics data and to determine the adsorption mechanism.

First- and second-order models

Equations (5) and (6) represent rate equations for first and second order:

$$\ln C_t = \ln C_o - K_1 t \quad (5)$$

$$\frac{1}{C_t} = K_2 t + \frac{1}{C_o} \quad (6)$$

where K_1 and K_2 are the first-order and the second-order adsorption rate constants (min^{-1}). Figure 7 shows a plot of $\ln C_t$ *versus t*, while Fig. 8 shows a plot of $1/C_t$ *versus t*.

Pseudo-first-order and pseudo-second-order models

The kinetics of adsorption can also be described using a pseudo-first-order or pseudo-second-order equation. While the model based on pseudo-first-order kinetics assumes binding to be a result of adsorption, that based on pseudo-second-order kinetics regards it as a consequence of chemical adsorption.[18] Equations (7) and (8) represent the linear relations of the pseudo-first-order and pseudo-second-order rate equations:

$$\ln(q_e - q_t) = \ln q_e - K_1 t \quad (7)$$

$$\frac{t}{q_t} = \frac{1}{K_2 q_e^2} + \frac{1}{q_e} t \quad (8)$$

where q_t represents the concentration of metal ions at time t (min) and q_e (mg g^{-1}) the concentration at equilibrium adsorbed by the adsorbing material. K_1 (min^{-1}) represents the pseudo-first-order rate constant, while K_2 (min^{-1}) represents the pseudo-second-order rate constant. supporting information, Fig. S2, shows a plot of $\ln(q_e - q_t)$ *versus t* while, supporting information, Fig. S3, shows a plot of t/q_t *versus t*.

Intraparticle diffusion model or Weber–Morris kinetic model

To better understand the mechanism of diffusion of the process of adsorption, the intraparticle diffusion model was investigated.[18] The intraparticle diffusion model is expressed by Eqn (9):

$$q_t = K_i t^{1/2} + C \quad (9)$$

where K_i (mg g^{-1} $min^{-1/2}$) represents the rate constant of the intraparticle diffusion and C, the intercept, relates to the boundary layer thickness.[52] If C is equal to zero, intraparticle diffusion will be the only controlling step. By contrast, values of $C \neq 0$ suggest that the adsorption process is partly complex and involves more than one resistance to diffusion.[53] In the intraparticle diffusion model, the diffusion of pores is supposed to be through sorption at the surfaces because the adsorbent is porous in nature.[54] The linear plot of q_t *versus* $t^{1/2}$ provided the descriptors for this model (supporting information, Fig. S4).

Table 1 presents the kinetic parameters and correlation coefficients. The model based on pseudo-second-order kinetics was thought appropriate in describing the adsorption of the metal ions given the higher correlation coefficients, which suggests that the process of adsorption is controlled by chemisorption rather than mass transport. The experimental value of q_e agrees very closely with the theoretical value predicted using a model based on pseudo-second-order kinetics. Results from several studies of the adsorption of Pb(II) on MNPs have demonstrated that the model based on pseudo-second-order kinetics fits best with the data obtained experimentally.[18,52]

Adsorption isotherm study

Effect of initial concentration of Pb(II) ions. The rate of adsorption depends on the initial concentration of the adsorbate (2–15 ppm), weight of adsorbent (10 mg), pH (6.5) and contact time (60 min). Thus, an important factor that controls effective adsorption is the concentration of the adsorbate. The adsorption of Pb(II) ions onto the adsorbent in relation to the initial concentration of Pb(II) ions is presented in Fig. 9(A). We observed that the removal efficiency of Pb(II) decreased as the Pb(II) concentration increased from 2 to 15 mg L^{-1}. The fast and high adsorption,

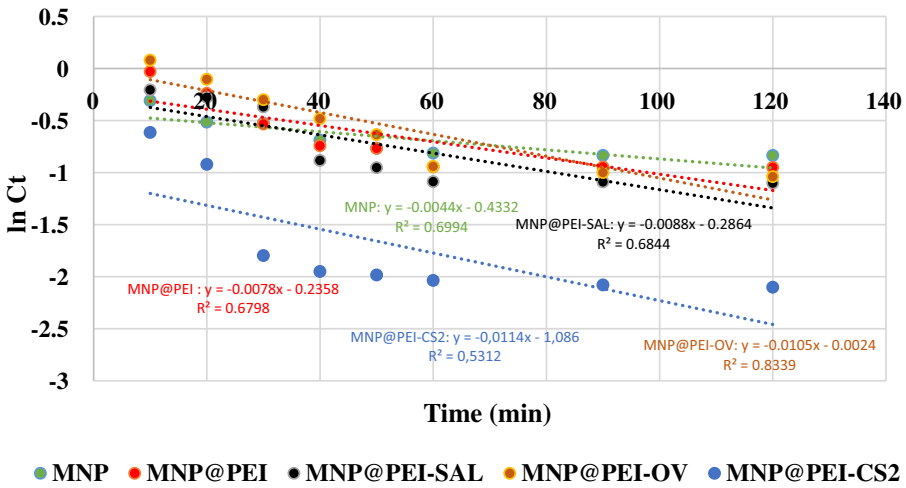

Figure 7. Model based on first-order kinetics for Pb(II) ion removal by MNPs, MNP@PEI, MNP@PEI-CS_2, MNP@PEI-SAL and MNP@PEI-OV.

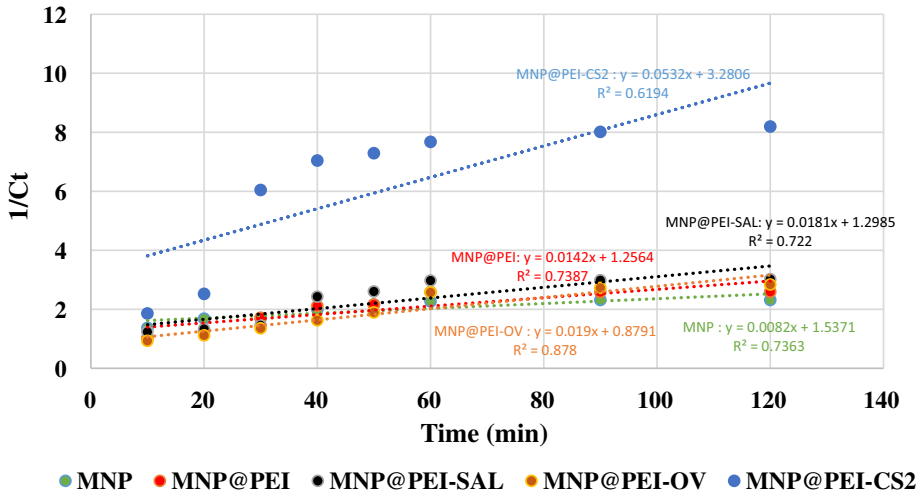

Figure 8. Model based on second-order kinetics for Pb(II) ion removal by MNPs, MNP@PEI, MNP@PEI-CS_2, MNP@PEI-SAL and MNP@PEI-OV.

Table 1. Kinetic parameters and correlation coefficients

Adsorbent		MNP	MNP@PEI	MNP@PEI-SAL	MNP@PEI-OV	MNP@PEI-CS_2
q_{exp} (mg g^{-1})		129.333	130.272	131.362	130.934	135.557
First-order model	K_1	0.44×10^{-2}	0.78×10^{-2}	0.88×10^{-2}	1.05×10^{-2}	1.14×10^{-2}
	R^2	0.6994	0.6798	0.6844	0.8339	0.5312
Second-order model	K_2	0.82×10^{-2}	1.42×10^{-2}	1.81×10^{-2}	1.90×10^{-2}	5.32×10^{-2}
	R^2	0.7363	0.7387	0.7220	0.878	0.6194
Pseudo-first-order model	K_1	11.76×10^{-2}	8.76×10^{-2}	9.94×10^{-2}	9.76×10^{-2}	9.13×10^{-2}
	q_e	64.097	42.674	75.596	153.361	25.868
	R^2	0.9025	0.9405	0.9068	0.8436	0.9133
Pseudo-second-order model	K_2	1.08×10^{-2}	0.57×10^{-2}	0.51×10^{-2}	0.35×10^{-2}	1.04×10^{-2}
	q_e	129.870	131.579	133.333	133.333	136.986
	R^2	1.0000	0.9999	0.9997	0.9997	0.9999
Intraparticle diffusion model	K_i	0.7473	1.4690	1.4206	1.9615	0.9719
	C	122.40	116.85	118.13	112.14	126.95
	R^2	0.7993	0.7636	0.7694	0.8825	0.6161

when the initial concentration is low, may be a consequence of the presence of several free sites on the surface of the adsorbing material which promoted interaction with the free Pb(II). Increasing the initial concentration of Pb(II) in the solution resulted in a reduction in the active sites on the surface of MNP@PEI-CS_2 and thus a decrease in adsorption.[55]

Adsorption isotherm models

To design the adsorption system and establish the relationship between the adsorbate and the adsorbent, the adsorption isotherm was investigated while temperature was kept constant. Adsorption isotherms permit the prediction of the capacity of adsorption of the adsorbent and to better explain the

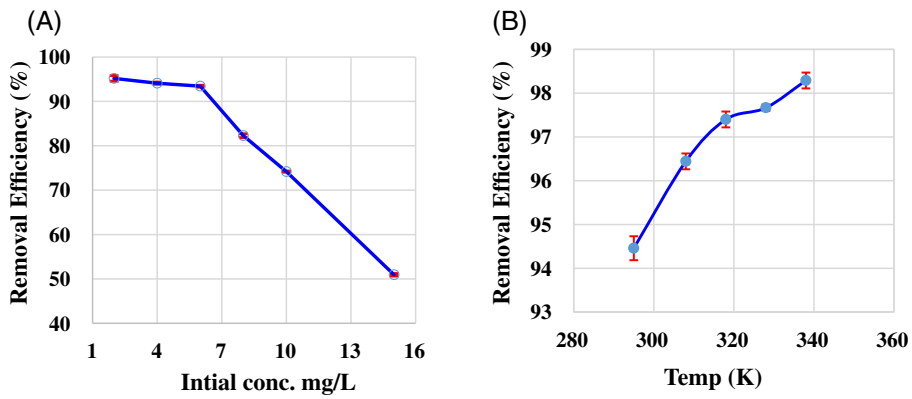

Figure 9. Removal efficiency of Pb^{2+} against (A) initial Pb^{2+} concentration and (B) temperature using MNP@PEI-CS_2.

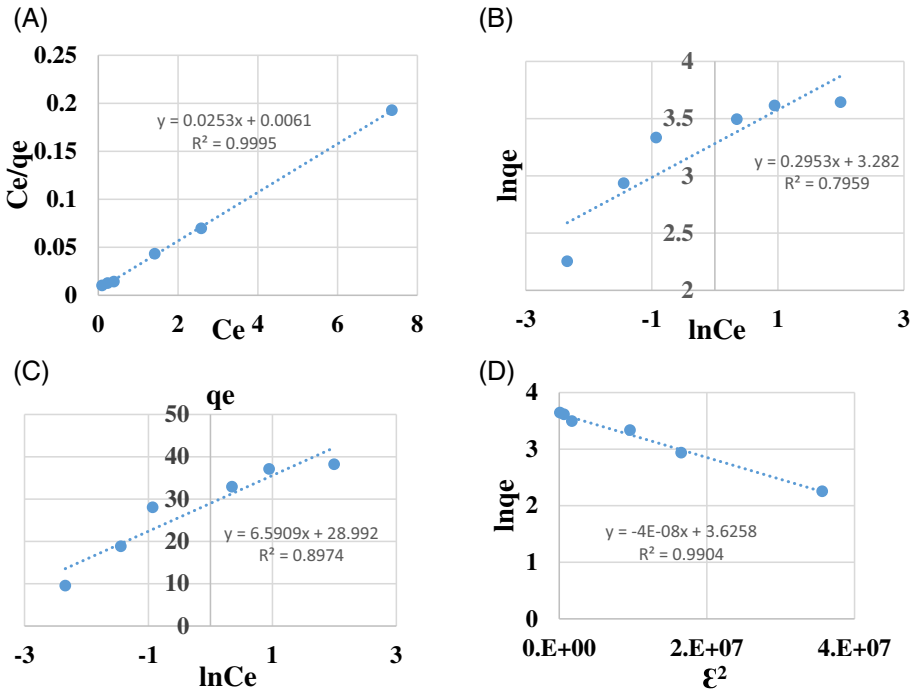

Figure 10. Isotherms of Pb(II) adsorption on MNP@PEI-CS_2: (A) Langmuir isotherm, (B) Freundlich isotherm, (C) Temkin isotherm and (D) D-R isotherm.

interaction between the adsorbent and heavy metal ions.[56] In this study, the Langmuir (Eqn (10)), Freundlich (Eqn (11)), Temkin (Eqn (12)) and Dubinin–Radushkevich (D-R) (Eqn (13)) isotherms were chosen to describe the equilibrium between the amounts of Pb(II) adsorbed on MNP@PEI-CS_2 (q_e) and Pb(II) concentration in the solution (C_e):

$$\frac{C_e}{q_e} = \frac{1}{q_{max} K_L} + \frac{1}{q_{max}} C_e \quad (10)$$

$$\ln q_e = \ln K_F + \frac{1}{n} \ln C_e \quad (11)$$

$$q_e = B_T \ln K_T + B_T \ln C_e \text{ where } B_T = \frac{RT}{b_T} \quad (12)$$

$$\ln q_e = \ln q_s - K_{D-R} \varepsilon^2 \quad (13)$$

where C_e (mg L^{-1}), q_e (mg L^{-1}) and q_{max} (mg g^{-1}) represent the concentration of Pb(II) at equilibrium, the quantity of Pb(II) adsorbed at equilibrium and the maximum capacity of uptake of the adsorbing material, respectively. K_L (L mg^{-1}) is a Langmuir constant that relates to the energy adsorbed; while the Freundlich constants n and K_F are related to the intensity of sorption and the capacity of sorption, respectively. K_T (L g^{-1}), b_T and B_T are the Temkin isotherm equilibrium binding constant, Temkin isotherm constant and a constant related to the heat of sorption (J mol^{-1}), respectively.[18,57] $K_{D\text{-}R}$ (mol^2 kJ^{-2}) is the D-R constant and ε (J mol^{-1}) shows the Polanyi potential,[58] q_s represents the theoretical isotherm saturation capacity (mg g^{-1}),[59] R represents the gas constant (8.314 J mol^{-1} K^{-1}) and T is the temperature at 298 K. Equation (14) permits the calculation of the mean free energy (E, kJ mol^{-1}):

$$E = \frac{1}{\sqrt{2\beta}} \text{ with } \beta = K_{D-R} \quad (14)$$

The E value may determine the nature of the adsorption: for instance, E in the range 8–16 kJ mol^{-1} means that the adsorption process is chemical in nature, while it is controlled by a physical process if E is below 8 kJ mol^{-1}. The isotherms or plots for the removal of Pb(II) by MNP@PEI-CS_2 under optimum conditions are shown in Fig. 10. The calculated E value (3.535 kJ mol^{-1}), in the range 8–16 kJmol^{-1}, obtained from the D-R model fitting parameters, indicates that the process of adsorption was physical.[60] Table 2 lists the isotherm constants and correlation coefficients. The Langmuir model fits better the experimental data, in comparison to the Temkin and Freundlich isotherm models, because of the higher correlation coefficients, suggesting a monolayer adsorption. This indicates that the surfaces are homogeneous and all adsorption sites are equivalent.[14,61] In order to evaluate how suitable the adsorbent is towards the adsorbate investigated, a separation factor constant (R_L) (Eqn (15)) was applied. The constant R_L (which is dimensionless) enables us to infer if the process of adsorption is favorable or not.

$$R_L = \frac{1}{1 + K_L C_o} \quad (15)$$

where K_L (L mg^{-1}) represents the Langmuir constant.

Thus, the magnitude of R_L indicates if the adsorption process is feasible[18] and also qualifies the isotherm type as either irreversible ($R_L = 0$), favorable ($0 < R_L < 1$), linear ($R_L = 1$) or unfavorable ($R_L > 1$).[62] The values of R_L presented in Table 2 indicate that Pb(II) adsorption by MNP@PEI-CS_2 is favorable.

Adsorption thermodynamics study

The spontaneity of the adsorption process using MNP@PEI-CS_2 adsorbent was described by thermodynamic parameters with a temperature variation from 295 to 338 K. Variation in the removal percentage of Pb(II) with temperature is shown in Fig. 9(B). Adsorption of Pb(II) ions on the magnetite adsorbent was found

Table 2. Descriptors of isotherms for Pb(II) adsorption on MNP@PEI-CS_2

Metal ion	q_{exp} (mg g^{-1})	Langmuir isotherm model				Freundlich isotherm model			Temkin isotherm model			D-R isotherm model		
		q_{max} (mg g^{-1})	K_L (L mg^{-1})	R^2	R_L	n	K_F (mg g^{-1})	R^2	b_T (J mol^{-1})	K_T (L g^{-1})	R^2	q_m (mg g^{-1})	K_{D-R} (mol^2 J^{-2})	R^2	E (kJ mol^{-1})
Pb(II)	38.19	39.52	4.147	0.99	0.0337	3.38	26.628	0.79	372.12	81.35	0.89	37.55	4×10^{-8}	0.99	3.535

to increase with increasing adsorption temperature since they gained energy in the system and their mobility increased. This indicated that the process of adsorption was endothermic, and could also possibly be a chemical adsorption process.[63] The parameters $\Delta H°$, $\Delta S°$ and $\Delta G°$ relating to the thermodynamics of the adsorption on MNP@PEI-CS_2 could be obtained from the process that depends on temperature. The values of $\Delta H°$ and $\Delta S°$ were calculated by applying Eqns (16)–(18)[52]:

$$\Delta G° = \Delta H° - T\Delta S° \tag{16}$$

$$\ln K_d = \frac{\Delta S°}{R} - \frac{\Delta H°}{RT} \tag{17}$$

$$K_d = \frac{C_o - C_e}{C_e} \cdot \frac{V}{m} \tag{18}$$

where K_d is the distribution coefficient at equilibrium, C_o (mg L^{-1}) the concentration at the origin, C_e (mg L^{-1}) the concentration at equilibrium, V the volume (mL), m the amount (g) of adsorbent, R the ideal gas constant (8.314 J mol^{-1} K^{-1}), T the temperature (K), $\Delta H°$ the enthalpy of adsorption, $\Delta G°$ the free energy change and $\Delta S°$ the entropy change. The calculated and estimated thermodynamic parameters are presented in Table 3. The higher the value of K_d, the more the sorbent material tends to be effective at sequestering the target species. Under experimental conditions, K_d is a direct measure of the affinity of a sorbent for the species being measured (and this may impact the value).[64] The distribution coefficient (K_d) values increased with an increase in temperature suggesting that the process of adsorption was endothermic in nature. The $\Delta G°$ values decreased with temperature rise. An indication of how feasible is the adsorption of metal ions on the adsorbent, as well as the spontaneity and thermodynamical favorability of the sorption process are given by the negative values of $\Delta G°$.[65]

While positive $\Delta H°$ values indicate an endothermic adsorption process, positive $\Delta S°$ values show that the 'degree of freedom' of the Pb(II) ions in the medium increases, suggesting that the concentration of the sorbate increases in the solid–liquid interface.

The adsorption of Pb(II) ions, as shown by the thermodynamic parameters, was found to be a non-spontaneous process at low temperatures, and spontaneous at high temperatures.

Regeneration and reusability study

The main objectives for the regeneration of adsorbents are: (i) to reinstate the capacity for adsorption of adsorbents that have been exhausted and (ii) to extract valuable metals that are found in the adsorbed phase.[66]

To evaluate the efficiency of the adsorbent, regeneration was conducted and the adsorbent (MNP@PEI-CS_2) was reused for three cycles. The regeneration study reveals that Pb(II) could totally be desorbed by 0.5 mol L^{-1} HCl. The Pb(II) removal efficiency was 94.1%, 91.2% and 90.1% for the first, second and third cycles (adsorption–desorption), respectively (Fig. 11), indicating the stability of the adsorbent in the process of desorption and good reusability. The decrease in the removal efficiency after regeneration in subsequent cycles may be due to the fact that the adsorbate could not be completely recovered from the adsorbent during the desorption process. Thus, these results suggest that the non-thermal desorption method was quite effective to retain the adsorbents and be reused for several cycles for the removal of Pb^{2+}.

The adsorbent structure was preserved after regeneration and was confirmed from FTIR spectra of the adsorbent before and

Table 3. Thermodynamics of Pb ion removal from aqueous solution by MNP@PEI-CS_2

		MNP@PEI-CS_2			
Metal	T (K)	K_d	$\Delta G°$ (kJ mol^{-1})	$\Delta H°$ (kJ mol^{-1})	$\Delta S°$ (J mol^{-1})
Pb(II)	295	340.89	−14.302	22.6265	125.5331
	308	542.15	−16.121		
	318	749.26	−17.500		
	328	837.24	−18.353		
	338	1149.28	−19.802		

Table 4. Comparison table of adsorption capacities for Pb(II) of various magnetic adsorbents

Adsorbent	Adsorption capacity (mg g^{-1})	Pb^{2+} (%RE)	Pb conc. (mg L^{-1})	pH	Time (min)	Ref.
3-Mercaptopropanic acid@PMNP	68.41	98	200	6.5	60	67
Ultrafine mesoporous Fe_3O_4 nanoparticles	85	96–97	10	5.5	20–30	68
Fe_3O_4@silica–xanthan gum	21.32	>99	28	6.0	60	69
Iron oxide nanoparticles	36.0	98	162	5.5	120	70
Fe_3O_4@SiO_2@						
2-Chloropyridine	61	94	10	5	20	71
3-Chloropyridazine	72	96				
2-Chloropyrazine	65	94				
4-Chloropyrimidine	65	93				
Fe_3O_4@Silica-MnO_2	33.6	94	24	4	30	72
MNP-polyethyleneimine	143	>99	100	6	60	73
Carboxyl-MNP	74.63	>99	10	5	30	74
MNP@PEI-CS_2	39.52	92	25	6.5	10	This work

after adsorption, and after desorption (supporting information, Fig. S5). The FTIR spectrum of MNP@PEI-CS_2 before adsorption shows a peak around 1632 cm^{-1} related to the C—N stretching vibration which shifted to a lower frequency after adsorption at around 1413 cm^{-1}. This indicates that Pb(II) was adsorbed on the MNP@PEI-CS_2. After the regeneration (after desorption), the peak (C—N) reappeared at *ca* 1632 cm^{-1} but with a decreased intensity. Similarly, the peak at around 3400 cm^{-1} due to NH_2 disappears after adsorption and reappears with lower intensity after desorption, indicating these groups were also involved in the adsorption process. Thus, the FTIR spectra of the adsorbent after regeneration support the finding that it is able to be regenerated and reused several times without significant loss.

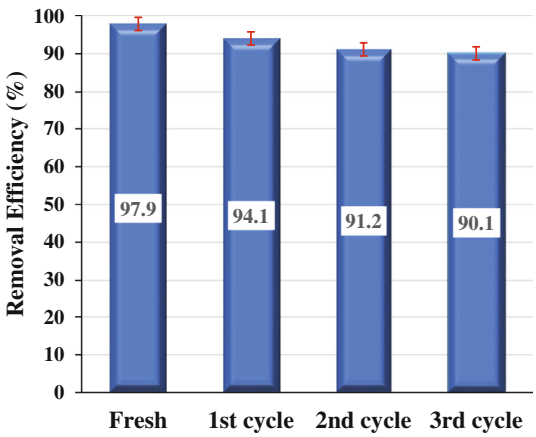

Figure 11. Adsorption–desorption cycles on MNP@PEI-CS_2.

Comparative study

The Pb(II) removal efficiency of CS_2-functionalized MNP@PEI in this present work was compared with that of other adsorbents in the literature as presented in Table 4. As can be seen, the removal efficiency of MNP@PEI-CS_2 is comparable to that of similar materials. In addition, this efficiency is achieved in a shorter time, indicating that our modified method is effective and practicable.

CONCLUSION

The present study has demonstrated that MNP@PEI decorated with a range of functional groups, namely salicylaldehyde, *o*-vanillin and CS_2, can be used as promising adsorbent materials for complexing and removing Pb(II) ions from aqueous solutions. Functionalization provides specific functional groups at the MNP@PEI surfaces for further bonding of different molecules to surfaces containing oxygen, nitrogen and sulfur functional groups on these surfaces to act as available adsorption sites. Therefore, functionalized MNPs have a high degree of interaction and ability to remove specific contaminants in contaminated water. The presence of a coating polymer (PEI) on the surface of the as-synthesized MNPs was demonstrated from FTIR spectra which equally identified the functional groups responsible for metal ion removal from aqueous solutions. Morphological observations through SEM and TEM showed nanoparticles of smooth surfaces with sizes ranging from 20 to 40 nm and with the average size of most of the particles being 30 nm in diameter. Batch

adsorption experiments disclosed a relatively high removal efficiency for Pb(II), which may be due to the coordination properties of PEI and the electrostatic interaction between Pb(II) and oxygen, nitrogen and sulfur functional groups on its surface. The MNP@PEI-CS_2 adsorbent demonstrates the highest adsorption capacity achieved within 50 min at 25 °C, which is most probably due to the strong affinity of Pb(II) ions for sulfur atoms. Factors that influence the batch adsorption process include the time of contact, temperature, dosage, solution pH and initial metal ion concentration. Experimental investigations optimized the conditions for the maximum removal of 25 mg L^{-1} Pb(II) ions to be 10 mg, 60 min contact time and a pH of 6.5.

The adsorption kinetics fit well the model based on pseudo-second-order kinetics and the Langmuir isotherm. The thermodynamic study indicated that the process of adsorption was endothermic and spontaneous and increasing the temperature promoted adsorption. Based on this study, the adsorbents could be satisfactorily used in practical applications for heavy metal ion removal from an aqueous environment due to the high capacity of adsorption coupled with the ease and rapidity of separation, avoiding the issues with centrifugation and filtration. The present work also shows that these adsorbents can be reused as highly efficient adsorbents for Pb(II) removal from aqueous solution.

ACKNOWLEDGEMENTS

This work was supported by the Organization for Women in Science for the Developing World (OWSD) and Swedish International Development Cooperation Agency (SIDA) for a sandwich postgraduate fellowship at the Catalysis Research Laboratory of the University of the Western Cape (South Africa) and the University of Yaounde I (Cameroon).

SUPPORTING INFORMATION

Supporting information may be found in the online version of this article.

REFERENCES

1 Assegide E, Alamirew T, Bayabil H, Dile YT, Tessema B and Zeleke G, Impacts of surface water quality in the Awash River basin, Ethiopia: a systematic review. *Front Water* **3**:1–15 (2022). https://doi.org/10.3389/frwa.2021.790900.
2 Bijekar S, Padariya HD, Yadav VK, Gacem A, Hasan MA, Awwad NS *et al.*, The state of the art and emerging trends in the wastewater treatment in developing nations. *Water* **14**:2537 (2022). https://doi.org/10.3390/w14162537.
3 Cho H-H, Wepasnick K, Smith BA, Bangash FK, Fairbrother DH and Ball WP, Sorption of aqueous Zn[II] and Cd[II] by multiwall carbon nanotubes: the relative roles of oxygen-containing functional groups and graphenic carbon. *Langmuir* **26**:967–981 (2010). https://doi.org/10.1021/la902440u.
4 Chen Z, Tang B, Niu Y, Chen H, Liu Y, Wang A *et al.*, Synthesis of silica supported thiosemicarbazide for Cu(II) and Zn(II) adsorption from ethanol: a comparison with aqueous solution. *Fuel* **286**:119287 (2021). https://doi.org/10.1016/j.fuel.2020.119287.
5 Das TK and Poater A, Review on the use of heavy metal deposits from water treatment waste towards catalytic chemical syntheses. *Int J Mol Sci* **22**:13383 (2021). https://doi.org/10.3390/ijms222413383.
6 Briffa J, Sinagra E and Blundell R, Heavy metal pollution in the environment and their toxicological effects on humans. *Heliyon* **6**:e04691 (2020). https://doi.org/10.1016/j.heliyon.2020.e04691.
7 Jia C, Junhong Z, Liling L, Xiyang K, Ran L, Chongtao C *et al.*, Novel magnetically separable anhydride-functionalized Fe_3O_4@SiO_2@PEI-NTDA nanoparticles as effective adsorbents: synthesis, stability and recyclable adsorption performance for heavy metal ions. *RSC Adv* **9**:9533–9545 (2019). https://doi.org/10.1039/c8ra10310k.
8 Collin MS, Venkatraman SK, Vijayakumar N, Kanimozhi V, Arbaaz SM, Stacey RG *et al.*, Bioaccumulation of lead (Pb) and its effects on human: a review. *J Hazard Mater Adv* **7**:100094 (2022). https://doi.org/10.1016/j.hazadv.2022.100094.
9 Jacob J, Karthik C, Saratale RG, Kumar S, Prabakar D, Kadirvelu K *et al.*, Biological approaches to tackle heavy metal pollution: a survey of literature. *J Environ Manage* **217**:56–70 (2018). https://doi.org/10.1016/j.jenvman.2018.03.077.
10 Pang FM, Kumar P, Teng TT, Mohd Omar AK and Wasewar K, Removal of lead, zinc and iron by coagulation–flocculation. *J Taiwan Inst Chem Eng* **42**:809–815 (2011). https://doi.org/10.1016/j.jtice.2011.01.009.
11 Lalmi A, Bouhidel K-E and Sahraoui B, Removal of lead from polluted waters using ion exchange resin with $Ca(NO_3)_2$ for elution. *Hydrometallurgy* **178**:287–293 (2018). https://doi.org/10.1016/j.hydromet.2018.05.009.
12 Chowdhury IR, Chowdhury S, Mazumder MAJ and al-Ahmed A, Removal of lead ions (Pb^{2+}) from water and wastewater: a review on the low-cost adsorbents. *Appl Water Sci* **12**:185 (2022). https://doi.org/10.1007/s13201-022-01703-6.
13 Yang K, Lou Z, Fu R, Zhou J, Xu J, Baig SA *et al.*, Multiwalled carbon nanotubes incorporated with or without amino groups for aqueous Pb(II) removal: comparison and mechanism study. *J Mol Liq* **260**:149–158 (2018). https://doi.org/10.1016/j.molliq.2018.03.082.
14 Gul Zaman H, Baloo L, Pendyala R, Singa PK, Ilyas SU and Kutty SR, Produced water treatment with conventional adsorbents and MOF as an alternative: a review. *Materials* **14**:7607 (2021). https://doi.org/10.3390/ma14247607.
15 Kavosi Rakati K, Mirzaei M, Maghsoodi S and Shahbazi A, Preparation and characterization of polyaniline modified chitosan embedded with ZnO-Fe_3O_4 for Cu(II) removal from aqueous solution. *Int J Biol Macromol* **130**:1025–1045 (2019). https://doi.org/10.1016/j.ijbiomac.2019.02.033.
16 Plohl O, Simonič M, Kolar K, Gyergyek S and Fras Zemljič L, Magnetic nanostructures functionalized with a derived lysine coating applied to simultaneously remove heavy metal pollutants from environmental systems. *Sci Tech Adv Mater* **22**:55–71 (2021). https://doi.org/10.1080/14686996.2020.1865114.
17 Mudhoo A and Sillanpää M, Magnetic nanoadsorbents for micropollutant removal in real water treatment: a review. *Environ Chem Lett* **19**:4393–4413 (2021). https://doi.org/10.1007/s10311-021-01289.
18 Liosis C, Papadopoulou A, Karvelas E, Karakasidis TE and Sarris IE, Heavy metal adsorption using magnetic nanoparticles for water purification: a critical review. *Materials* **14**:7500 (2021). https://doi.org/10.3390/ma14247500.
19 Luan L, Tang B, Liu Y, Wang A, Zhang B, Xu W *et al.*, Selective capture of Hg(II) and Ag(I) from water by sulfur-functionalized polyamidoamine dendrimer/magnetic Fe_3O_4 hybrid materials. *Sep Purif Technol* **257**:117902 (2021). https://doi.org/10.1016/j.seppur.2020.117902.
20 Chai WS, Cheun JY, Kumar PS, Mubashir M, Majeed Z, Banat F *et al.*, A review on conventional and novel materials towards heavy metal adsorption in wastewater treatment application. *J Cleaner Prod* **296**:126589 (2021). https://doi.org/10.1016/j.jclepro.2021.126589.
21 Wang B, Wu K, Liu T, Cheng Z, Liu Y, Liu Y *et al.*, Feasible synthesis of bifunctional polysilsesquioxane microspheres for robust adsorption of Hg(II) and Ag(I): behavior and mechanism. *J Hazard Mater* **442**:130121 (2023). https://doi.org/10.1016/j.jhazmat.2022.130121.
22 Zhu N, Ji H, Yu P, Niu J, Farooq MU, Akram MW *et al.*, Surface modification of magnetic iron oxide nanoparticles. *Nanomaterials* **8**:810 (2018). https://doi.org/10.3390/nano8100810.
23 Wang X, Niu D, Hu C and Li P, Polyethyleneimine-based nanocarriers for gene delivery. *Curr Pharm Des* **21**:6140–615642 (2015). https://doi.org/10.2174/1381612821666151027152907.
24 Lungu CN, Diudea MV, Putz MV and Grudziński IP, Linear and branched PEIs (polyethylenimines) and their property space. *Int J Mol Sci* **17**:555 (2016). https://doi.org/10.3390/ijms17040555.
25 Shukla S, Khan R and Daverey A, Synthesis and characterization of magnetic nanoparticles, and their applications in wastewater treatment: a review. *Environ Technol Innov* **24**:101924 (2021). https://doi.org/10.1016/j.eti.2021.101924.
26 Lin C-R, Ivanova OS, Petrov DA, Sokolov AE, Chen Y-Z, Gerasimova MA *et al.*, Amino-functionalized Fe_3O_4@SiO_2 core-shell magnetic

nanoparticles for dye adsorption. *Nanomaterials* **11**:2371 (2021). https://doi.org/10.3390/nano1192371.
27 Aeineh N, Salehi F, Akrami M, Nemati F, Alipour M, Ghorbani M *et al.*, Glutathione conjugated polyethylenimine on the surface of Fe_3O_4 magnetic nanoparticles as a theranostic agent for targeted and controlled curcumin delivery. *J Biomater Sci Polym Ed* **29**:1109–1125 (2018). https://doi.org/10.1080/09205063.2018.1427013.
28 Yu C, Li Q, Tian J, Zhan H, Zheng X, Wang S *et al.*, A facile preparation of immobilized naringinase on polyethyleneimine-modified Fe_3O_4 magnetic nanomaterials with high activity. *RSC Adv* **11**:14568–14577 (2021). https://doi.org/10.1039/D1RA01449H.
29 Kothavale VP, Sharma A, Dhavale RP, Chavan VD, Shingte SR, Selyshchev O *et al.*, Hyperbranched amino modified magnetic nanoparticles for simultaneous removal of heavy metal ions from aqueous solutions. *Mater Chem Phys* **292**:126792 (2022). https://doi.org/10.1016/j.matchemphys.2022.126792.
30 Jia C, Zhao J, Lei L, Kang X, Lu R, Chen C *et al.*, Novel magnetically separable anhydride-functionalized Fe_3O_4@SiO_2@PEI-NTDA nanoparticles as effective adsorbents: synthesis, stability and recyclable adsorption performance for heavy metal ions. *RSC Adv* **9**:9533–9545 (2019).
31 Culita DC, Simonescu CM, Patescu R-E, Dragne M, Stanica N and Oprea O, O-vanillin functionalized mesoporous silica-coated magnetite nanoparticles for efficient removal of Pb(II) from water. *J Solid State Chem* **238**:311–320 (2016). https://doi.org/10.1016/j.jssc.2016.04.003.
32 Gallio AE, Brustolin L, Pettenuzzo N and Fregona D, Binuclear heteroleptic Ru(III) dithiocarbamate complexes: a step towards tunable antiproliferative agents. *Inorganics* **10**:37 (2022). https://doi.org/10.3390/inorganics10030037.
33 Angeloski A, Gentle AR, Scott JA, Cortie MB, Hook JM, Westerhausen MT *et al.*, From lead(II) dithiocarbamate precursors to a fast response PBS positive temperature coefficient thermistor. *Inorg Chem* **57**:2132–2140 (2018). https://doi.org/10.1021/acs.inorgchem.7b03009.
34 Jafarinejad S, Faraji M, Norouzi Z and Aliabad J, Application of sulfur-modified magnetic nanoparticles for cadmium removal from aqueous solutions. *J Water Environ Nanotechnol* **3**:58–69 (2018). https://doi.org/10.22090/jwent.2018.01.006.
35 Oladipo SD, Omondi B and Mocktar C, Co(III) *n,n′*-diarylformamidine dithiocarbamate complexes: synthesis, characterization, crystal structures and biological studies. *Appl Organomet Chem* **34**:e5610 (2020). https://doi.org/10.1002/aoc.5610.
36 Ferjani H and Onwudiwe DC, Synthesis, structural, thermal, and Hirshfeld surface analysis of In(III) tris(N-methyl-N-phenyl dithiocarbamate). *Inorganics* **10**:146 (2022). https://doi.org/10.3390/inorganics10100146.
37 Sun S, Zeng H, Robinson DB, Raoux S, Rice PM, Wang SX *et al.*, Monodisperse MFe_2O_4 (M = Fe, Co, Mn) nanoparticles. *J Am Chem Soc* **126**:273–279 (2003). https://doi.org/10.1021/ja0380852.
38 Zhou ZH, Wang J, Liu X and Chan HS, Synthesis of Fe_3O_4 nanoparticles from emulsions. *J Mater Chem* **11**:1704–1709 (2001). https://doi.org/10.1039/b100758k.
39 Masjedi A, Askarizadeh E and Baniyaghoob S, Magnetic nanoparticles surface-modified with tridentate ligands for removal of heavy metal ions from water. *Mater Chem Phys* **249**:122917 (2020). https://doi.org/10.1016/j.matchemphys.2020.
40 Zaman Brohi RO, Khuhawar MY and Mahar RB, Graphene oxide functionalized with a Schiff base for the removal of Pb(II) ions from contaminated water: experimental and modeling approach. *J Chem Technol Biotechnol* **95**:1694–1704 (2020). https://doi.org/10.1002/jctb.6362.
41 Alterary SS and AlKhamees A, Synthesis, surface modification, and characterization of Fe_3O_4@SiO_2 core@shell nanostructure. *Green Process Syn* **10**:384–391 (2021). https://doi.org/10.1515/gps-2021-0031.
42 Lesiak B, Rangam N, Jiricek P, Gordeev I, Tóth J, Kövér L *et al.*, Surface study of Fe_3O_4 nanoparticles functionalized with biocompatible adsorbed molecules. *Front Chem* **7**:642 (2019). https://doi.org/10.3389/fchem.2019.00642.
43 Bhandari R, Gupta P, Dziubla T and Hilt JZ, Single step synthesis, characterization and applications of curcumin functionalized iron oxide magnetic nanoparticles. *Mater Sci Eng C* **67**:59–64 (2016). https://doi.org/10.1016/j.msec.2016.04.093.
44 Solný T, Ptáček P, Opravil T, Dlabajová L, Březina M, Másilko J *et al.*, Preparation of magnetic nanoparticles by one step synthesis with morphology of particles changed based on time of reaction and temperature treatment. *J Exp Nanosci* **16**:1–10 (2020). https://doi.org/10.1080/17458080.2020.1844880.
45 Guo C, Wang Y, Wang F and Wang Y, Adsorption performance of amino functionalized magnetic molecular sieve adsorbent for effective removal of lead ion from aqueous solution. *Nanomaterials* **11**:2353 (2021). https://doi.org/10.3390/nano11092353.
46 Elkhaleefa A, Ali IH, Brima EI, Shigidi I, Elhag AB and Karama B, Evaluation of the adsorption efficiency on the removal of lead(II) ions from aqueous solutions using *Azadirachta indica* leaves as an adsorbent. *Processes* **9**:559 (2021). https://doi.org/10.3390/pr9030559.
47 Tran CV, Quang DV, Nguyen Thi HP, Truong TN and La DD, Effective removal of Pb(II) from aqueous media by a new design of Cu-Mg binary ferrite. *ACS Omega* **5**:7298–7306 (2020). https://doi.org/10.1021/acsomega.9b04126.
48 Pickering KL, Raa Khimi S and Ilanko S, The effect of silane coupling agent on iron sand for use in magnetorheological elastomers part 1: surface chemical modification and characterization. *Composites Part A* **68**:377–386 (2015). https://doi.org/10.1016/j.compositesa.2014.10.005.
49 Tighadouini S, Radi S, Ferbinteanu M and Garcia Y, Highly selective removal of Pb(II) by a pyridylpyrazole-*β*-ketoenol receptor covalently bonded onto the silica surface. *ACS Omega* **4**:3954–3964 (2019). https://doi.org/10.1021/acsomega.8b03642.
50 Fu W and Huang Z, One-pot synthesis of a two-dimensional porous Fe_3O_4/poly($C_3N_3S_3$) network nanocomposite for the selective removal of Pb(II) and Hg(II) from synthetic wastewater. *ACS Sustainable Chem Eng* **6**:14785–14794 (2018). https://doi.org/10.1021/acssuschemeng.8b03320.
51 Qasem NAA, Mohammed RH and Lawal DU, Removal of heavy metal ions from wastewater: a comprehensive and critical review. *Clean Water* **4**:36 (2021). https://doi.org/10.1038/s41545-021-00127-0.
52 Azarudeen RS, Ahamed MA, Subha R and Burkanudeen AR, Heavy and toxic metal ion removal by a novel polymeric ion-exchanger: synthesis, characterization, kinetics and equilibrium studies. *J Chem Technol Biotechnol* **90**:2170–2179 (2014). https://doi.org/10.1002/jctb.4528.
53 Kakavandi B, Esrafili A, Mohseni-Bandpi A, Jonidi Jafari A and Rezaei KR, Magnetic Fe_3O_4@C nanoparticles as adsorbents for removal of amoxicillin from aqueous solution. *Water Sci Technol* **69**:147–155 (2014). https://doi.org/10.2166/wst.2013.568.
54 Rahman MS and Sathasivam KV, Heavy metal adsorption onto *Kappaphycus* sp. from aqueous solutions: the use of error functions for validation of isotherm and kinetics models. *Biomed Res Int* **2015**:1–13 (2015). https://doi.org/10.1155/2015/126298.
55 El-Arish NAS, Zaki RSRM, Miskan SN, Setiabudi HD and Jaafar NF, Adsorption of Pb(II) from aqueous solution using alkaline-treated natural zeolite: process optimization analysis. *Total Environ Res Themes* **3–4**:100015 (2022). https://doi.org/10.1016/j.totert.2022.100015.
56 Somu P, Kannan U and Paul S, Biomolecule functionalized magnetite nanoparticles efficiently adsorb and remove heavy metals from contaminated water. *J Chem Technol Biotechnol* **94**:2009–2022 (2019). https://doi.org/10.1002/jctb.5984.
57 Rápó E and Tonk S, Factors affecting synthetic dye adsorption; desorption studies: a review of results from the last five years (2017–2021). *Molecules* **26**:5419 (2021). https://doi.org/10.3390/molecules26175419.
58 Mohamed SK, Alazhary AM, Al-Zaqri N, Alsalme A, Alharthi FA and Hamdy MS, Cost-effective adsorbent from arabinogalactan and pectin of cactus pear peels: kinetics and thermodynamics studies. *Int J Biol Macromol* **150**:941–947 (2020). https://doi.org/10.1016/j.ijbiomac.2019.11.187.
59 Jakobek L, Matić P, Kraljević Š, Ukić Š, Benšić M and Barron AR, Adsorption between quercetin derivatives and *β*-glucan studied with a novel approach to modeling adsorption isotherms. *Appl Sci* **10**:1637 (2020). https://doi.org/10.3390/app10051637.
60 Niu Y, Yang J, Qu R, Gao Y, Du N, Chen H *et al.*, Synthesis of silica-gel-supported sulfur-capped PAMAM dendrimers for efficient Hg(II) adsorption: experimental and DFT study. *Ind Eng Chem Res* **55**:3679–3688 (2016). https://doi.org/10.1021/acs.iecr.6b00172.
61 Hou L, Qin G, Qu Y, Yang C, Rao X, Gao Y *et al.*, Fabrication of recoverable magnetic composite material based on graphene oxide for fast removal of lead and cadmium ions from aqueous solution. *J Chem Technol Biotechnol* **96**:1345–1357 (2021). https://doi.org/10.1002/jctb.6655.
62 Moradi A, Najafi Moghadam P, Hasanzadeh R and Sillanpää M, Chelating magnetic nanocomposite for the rapid removal of Pb(II) ions

from aqueous solutions: characterization, kinetic, isotherm and thermodynamic studies. *RSC Adv* **7**:433–448 (2017). https://doi.org/10.1039/C6RA26356A.
63 Adegoke HI, Adekola FA, Olowookere IT and Yaqub AL, Thermodynamic studies on adsorption of lead(II) ion from aqueous solution using magnetite, activated carbon and composites. *J Appl Sci Environ Manag* **21**:440 (2017). https://doi.org/10.4314/jasem.v21i3.5.
64 Warner CL, Addleman RS, Cinson AD, Droubay TC, Engelhard MH, Nash MA *et al.*, High-performance, superparamagnetic, nanoparticle-based heavy metal sorbents for removal of contaminants from natural waters. *ChemSusChem* **21**:749–757 (2010). https://doi.org/10.1002/cssc.201000027.
65 Bagbi Y, Sarswat A, Mohan D, Pandey A and Solanki PR, Lead and chromium adsorption from water using L-cysteine functionalized magnetite (Fe_3O_4) nanoparticles. *Sci Rep* **7**:7672 (2017). https://doi.org/10.1038/s41598-017-03380-x.
66 Lofrano G, Carotenuto M, Libralato G, Domingos RF, Markus A, Dini L *et al.*, Polymer functionalized nanocomposites for metals removal from water and wastewater: an overview. *Water Res* **92**:22–37 (2016). https://doi.org/10.1016/j.watres.2016.01.033.
67 Ali I, Peng C and Naz I, Removal of lead and cadmium ions by single and binary systems using phytogenic magnetic nanoparticles functionalized by 3-marcaptopropanic acid. *Chin J Chem Eng* **27**:949–964 (2019).
68 Fato FP, Li D-W, Zhao L-J, Qiu K and Long Y-T, Simultaneous removal of multiple heavy metal ions from river water using ultrafine mesoporous magnetite nanoparticles. *ACS Omega* **4**:7543–7549 (2019). https://doi.org/10.1021/acsomega.9b00731.
69 Peng X, Xu F, Zhang W, Wang J, Zeng C, Niu M *et al.*, Magnetic Fe_3O_4@silica–xanthan gum composites for aqueous removal and recovery of Pb^{2+}. *Colloids Surf A* **443**:27–36 (2014). https://doi.org/10.1016/j.colsurfa.2013.10.062.
70 Nashaat N, Rapid removal and recovery of Pb(II) from wastewater by magnetic nanoadsorbents. *J Hazard Mater* **184**:538–546 (2010).
71 Chen D, Awut T, Liu B, Ma Y, Wang T and Nurulla I, Functionalized magnetic Fe_3O_4 nanoparticles for removal of heavy metal ions from aqueous solutions. *e-Polymers* **16**:313–322 (2016). https://doi.org/10.1515/epoly-2016-0043.
72 Zhang H, Chen S, Shan Y, Qian X, Yang Y and Wang J, Highly effective lead ion adsorption by manganese-dioxide-supported core-shell structured magnetite. *Front Environ Sci* **10**:925205 (2022). https://doi.org/10.3389/fenvs.2022.925205.
73 Jiang H, Sun M, Xu J, Lu A and Shi Y, Magnetic Fe_3O_4 nanoparticles modified with polyethyleneimine for the removal of Pb(II). *Clean* **44**:1146–1153 (2016). https://doi.org/10.1002/clen.201500632.
74 Shi J, Li H, Lu H and Zhao X, Use of carboxyl functional magnetite nanoparticles as potential sorbents for the removal of heavy metal ions from aqueous solution. *J Chem Eng Data* **60**:2035–2041 (2015). https://doi.org/10.1021/je5011196.